Uncovering Conformal Symmetry in the 3D Ising Transition: State-Operator Correspondence from a Quantum Fuzzy Sphere Regularization

Wei Zhu[1,2,*] Chao Han,[2,1] Emilie Huffman,[3] Johannes S. Hofmann,[4] and Yin-Chen He[3,†]

[1]*School of Science, Westlake University, Hangzhou 310030, China*
[2]*Westlake Institute of Advanced Study, Westlake University, Hangzhou 310024, China*
[3]*Perimeter Institute for Theoretical Physics, Waterloo, Ontario N2L 2Y5, Canada*
[4]*Department of Condensed Matter Physics, Weizmann Institute of Science, Rehovot 76100, Israel*

The 3D Ising transition, the most celebrated and unsolved critical phenomenon in nature, has long been conjectured to have emergent conformal symmetry, similar to the case of the 2D Ising transition. Yet, the emergence of conformal invariance in the 3D Ising transition has rarely been explored directly, mainly due to unavoidable mathematical or conceptual obstructions. Here, we design an innovative way to study the quantum version of the 3D Ising phase transition on spherical geometry, using the "fuzzy (non-commutative) sphere" regularization. We accurately calculate and analyze the energy spectra at the transition, and explicitly demonstrate the state-operator correspondence (i.e., radial quantization), a fingerprint of conformal field theory. In particular, we identify 13 parity-even primary operators within a high accuracy and two parity-odd operators that were not known before. Our result directly elucidates the emergent conformal symmetry of the 3D Ising transition, a conjecture made by Polyakov half a century ago. More importantly, our approach opens a new avenue for studying 3D conformal field theories by making use of the state-operator correspondence and spherical geometry.

Subject Areas: Condensed Matter Physics,
Statistical Physics, String Theory

I. INTRODUCTION

Symmetry is one of the most important organizing principles in physics. As is well known, symmetries present microscopically [e.g., condensed matter systems, ultraviolet (UV) Lagrangians] can be spontaneously broken at low energies, giving rise to various distinct phases of matter such as crystals and magnets. Conversely and rather unexpectedly, symmetries absent microscopically can emerge at low energies, and such a phenomenon is called emergent symmetry. One prominent example is the order-disorder phase transition of the 2D Ising model, for which Polyakov discovered emergent conformal symmetry in 1970 [1], 26 years after Onsager's exact solution [2].

Polyakov's remarkable discovery of emergent conformal symmetry in the 2D Ising transition gave birth to conformal field theory (CFT) [3], a class of quantum field theories with profound applications in various fields of physics

including statistical mechanics, quantum condensed matter, string theory, and quantum gravity. In statistical physics, it is a common belief that many universality classes of (classical and quantum) phase transitions are captured by CFTs; however, this has not been proven for 3D transitions [4]. The emergence of conformal symmetry at phase transitions is not only aesthetically beautiful, but also useful in understanding the properties of these transitions, such as computing experimentally measurable critical exponents. In 2D the (local) conformal symmetry has an infinite-dimensional algebra, and it makes many 2D CFTs exactly solvable [3,7]. In $d > 2$ dimensions, there is only a finite-dimensional (global) conformal symmetry, i.e., $SO(d + 1, 1)$, with which one is not able to analytically solve CFTs as in 2D. Therefore, CFTs beyond 2D are rather poorly understood, with their solutions remaining outstanding for decades despite their broad appeal to physics and mathematics.

Historically, the study of lattice models for 2D classical phase transitions and their quantum cousins ($1 + 1D$ quantum phase transitions) played a key role in the discovery and understanding of 2D CFTs [1,2,8]. Similar progress in the study of conformal symmetry for $d \geq 3$ dimensional theories, however, has stalled due to the natural limitation of the lattice formulation. There are plenty of papers studying 3D phase transitions on the lattice, e.g., computing critical

*zhuwei@westlake.edu.cn
†yhe@perimeterinstitute.ca

exponents. However, the perspective of conformal symmetry has rarely been explored [9–14]. The conformal symmetry of a d-dimensional CFT is most transparent in geometries such as $\mathbb{R}^d$, S^d, as well as $S^{d-1} \times \mathbb{R}$. In particular, CFTs on $S^{d-1} \times \mathbb{R}$ obey a property called state-operator correspondence (i.e., radial quantization), which is a direct consequence of conformal symmetry [8]. Specifically, for a quantum Hamiltonian defined on sphere S^{d-1}, its eigenstates are in one-to-one correspondence with the scaling operators (including primary and descendant operators) of the infrared (IR) CFT. Moreover, the energy gaps of these eigenstates are proportional to the scaling dimensions of their corresponding scaling operators [15]. This nice feature can be used to explore various properties of CFTs, including scaling dimensions of operators, operator product expansion coefficients, and even operator algebras [8]. For 2D CFTs, $S^1 \times \mathbb{R}$ is very natural as one just needs to study a $1 + 1$D quantum lattice model defined on a 1D periodic chain (i.e., S^1) [16–19]. However, simulating lattice models of $d \geq 3$ dimensional CFTs on $S^{d-1} \times \mathbb{R}$ will be problematic, because a regular lattice cannot be put on a sphere $S^{d-1 \geq 2}$ due to its nontrivial curvature [20]. While efforts have nevertheless been made to discretize the sphere, no signature of state-operator correspondence has been found so far [21,22].

To overcome this geometric obstacle, in this paper we are pursuing a different direction; namely, we fuzzify a sphere [23]. Specifically, we study a $2 + 1$D quantum Ising transition defined on a fuzzy (noncommutative) sphere in light of Landau level regularization [24]. As a result of this innovative discretization, we observe almost perfect state-operator correspondence in surprisingly small system sizes. We use exact diagonalization to calculate properties of the $2 + 1$D Ising transition for up to 16 effective spins, and we find its low-lying eigenstates (up to 70 lowest states) split into representations of the 3D conformal symmetry (i.e., conformal multiplets), hence directly demonstrating the emergence of conformal symmetry. Among these low-energy states, we find 15 conformal primary states, most of which have not been discovered in any previous model studies of the 3D Ising transition. Specifically, we find 13 parity-even primaries, whose scaling dimensions agree well with state-of-the-art conformal bootstrap results [25,26] with discrepancies smaller than 1.6%. We also identify two parity-odd primaries which were unknown before.

Our observations directly verify conformal symmetry for the 3D Ising transition, which was conjectured by Polyakov 50 years ago [1]. Before our results, the most compelling evidence for the 3D Ising transition being conformal was from numerical conformal bootstrap [25–29], which assumes conformal symmetry and found critical exponents close to the values obtained by various methods such as Monte Carlo simulation [30,31] and measured by experiments [32]. In addition, there was an effort [14] to justify the conformal invariance of the 3D Ising by showing that the virial current [5,6] operator does not exist [33]. Our

obtained operator spectrum from the state-operator correspondence indeed convincingly shows that the 3D Ising transition does not have the virial current, which is a structural explanation of the 3D Ising being conformal [35]. A major surprise of our results is that an incredibly small system size (8–16 total spins) is already enough to yield accurate conformal data of the 3D Ising CFT. So we expect this approach to open a new avenue for studying higher dimensional phase transitions and CFTs. Firstly, there is a zoo of universalities that can be studied using our approach, which is amenable to various numerical techniques such as exact diagnolization (ED), density-matrix renormalization group (DMRG), and determinantal Monte Carlo. This offers an opportunity to tackle many open questions regarding phase transitions, critical phases, and CFTs. Secondly, a number of new universal quantities can be computed once the 3D CFT is simulated on a sphere, such as operator product expansion coefficients, F (of F theorem) [36–39], and the spherical binder ratio [40], just to name a few.

The paper is organized as follows. In Sec. II A, we review background knowledge including the radial quantization of CFTs and the state-operator correspondence. The spherical Landau level quantization and related fuzzy sphere are discussed in Sec. II B. Readers familiar with these topics can skip some of these subsections. In Sec. III, we formulate spherical Landau levels to regularize the 3D Ising transition on a fuzzy sphere. A global quantum phase diagram is presented. In Sec. IV, we present the low-lying energy spectra at the phase transition point and analyze their one-to-one correspondence with the scaling operators as predicted by the Ising CFT. This is the main result of this paper. And last, we present a discussion and outlook in Sec. V. Appendixes A–D contains more details about the formalism and numerical data including the complete spectrum of $N = 4$ electrons.

II. REVIEW OF BACKGROUND

A. Radial quantization of CFTs: State-operator correspondence

In this section we review some basics of radial quantization, and for an elaborated discussion we refer the readers to CFT lecture notes such as those in Refs. [7,41].

The conformal group in d dimensions $SO(d + 1, 1)$ is generated by d-dimensional translations $P_\mu = i\partial_\mu$, d-dimensional Lorentz rotations $M_{\mu\nu} = i(x_\mu \partial_\nu - x_\nu \partial_\mu)$, dilatations $D = ix^\mu \partial_\mu$, and special conformal transformations $K_\mu = i[2x_\mu(x^\nu \partial_\nu) - x^2 \partial_\mu]$. From the operator point of view, a CFT can be thought of as a theory whose operators form an infinite-dimensional representation of the conformal group. Specifically, one can write CFT operators $\{\hat{O}_\alpha\}$ as eigenoperators (i.e., irreducible representations) of the dilatation and Lorentz rotation $SO(d)$. In particular, the eigenvalue Δ of dilatation is called the scaling dimension of the operator, and it corresponds to the

exponent in the power law correlation function of the operator, e.g., $\langle O(x)O(0)\rangle \sim 1/|x|^{2\Delta}$. One can further categorize operators into primary operators and descendant operators: (1) primary operators are operators that are annihilated by the special conformal transformation K_μ; (2) descendant operators are not annihilated by K_μ, and all of them can be obtained by applying translations P_μ (multiple times) to the primary operators. Therefore, one can organize CFT operators as primary operators and their descendants, and each primary and its descendants form a set of operators called a conformal multiplet [42]. A CFT has an infinite number of primary operators, which makes it hard to tackle theoretically. A major task of solving a CFT is thus to obtain its low-lying (if not full) spectrum of primary operators.

To facilitate later analysis of our numerical results, we elaborate a bit more about the operator contents of a 3D CFT. In 3D the Lorentz rotation group is the familiar SO(3) group, all the irreducible representations of which are rank-ℓ symmetric traceless representations, i.e., spin-ℓ representations. So all (primary and descendant) operators have two quantum numbers (Δ, ℓ). A primary operator O with quantum number $\ell = 0$ is called a scalar operator, and any of its descendants can be written as

$$\partial_{\nu_1}\cdots\partial_{\nu_j}\Box^n O, \qquad n, j \geq 0, \qquad (1)$$

with quantum number $(\Delta + 2n + j, j)$. We note $\Box = \partial^2$. Here and hereafter all the free indices are symmetrized with the trace subtracted. The descendants of a spin-ℓ primary operator $O_{\mu_1\cdots\mu_\ell}$ are a bit more complicated as there are two different types. The first type can be written as

$$\partial_{\nu_1}\cdots\partial_{\nu_j}\partial_{\mu_1}\cdots\partial_{\mu_i}\Box^n O_{\mu_1\cdots\mu_\ell}, \qquad (2)$$

with quantum number $(\Delta + 2n + j + i, \ell + j - i)$ for $\ell \geq i \geq 0$, $n, j \geq 0$. Here and hereafter the repeated indices shall be contracted. The other type involves the ε tensor of SO(3), and can be written as

$$\varepsilon_{\mu_l\rho\tau}\partial_\rho\partial_{\nu_1}\cdots\partial_{\nu_j}\partial_{\mu_1}\cdots\partial_{\mu_i}\Box^n O_{\mu_1\cdots\mu_\ell}, \qquad (3)$$

with quantum number $(\Delta + 2n + j + i + 1, \ell + j - i)$ for $\ell - 1 \geq i \geq 0$, $n, j \geq 0$. We note that the ε tensor alters spacetime parity symmetry of $O_{\mu_1\cdots\mu_\ell}$.

We also remark that conserved operators (i.e., global symmetry current J_μ and energy momentum tensor $T_{\mu\nu}$) should be treated a bit differently, because they satisfy the conservation equations $\partial_\mu J_\mu = 0$ and $\partial_\mu T_{\mu\nu} = 0$. Therefore, their descendants in Eqs. (2) and (3) should have $i = 0$ [43].

Now we turn to the state perspective of CFTs. To define states of a CFT, we first need to quantize it, or in other words, find a Hilbert space construction of it. A quantum phase transition, namely, a quantum Hamiltonian realization of a d-dimensional CFT in $d - 1$ space dimensions, can be viewed as a way to quantize the CFT. The states of

the CFT are nothing but the quantum Hamiltonian's eigenstates. Formally, the quantization of CFTs can be more general than quantum phase transitions. Specifically, one can foliate d-dimensional spacetime into $(d - 1)$-dimensional surfaces, and each leaf of the foliation is endowed with its own Hilbert space. One convenient quantization is radial quantization, which has the d-dimensional Euclidean space $\mathbb{R}^d$ foliated to $S^{d-1} \times \mathbb{R}$, as shown in the left-hand side of Fig. 1. In the radial quantization, the SO(d) Lorentz rotation acts on the S^{d-1} sphere, while the dilatation acts as the scaling of sphere radius. Therefore, the states defined on the foliation S^{d-1} have well-defined quantum numbers of SO(d) rotation and dilatation, and they are indeed in one-to-one correspondence with operators of the CFT, dubbed as *state-operator correspondence*.

For a quantum Hamiltonian realization, the radial quantization described above is not natural, and instead one may want a quantization scheme that has an identical Hilbert space on each leaf of foliation. A quantum Hamiltonian is usually defined on the $M^{d-1} \times \mathbb{R}$ manifold: $\mathbb{R}$ is the time direction, while M^{d-1} is a $(d - 1)$-dimensional space manifold (e.g., sphere, torus, etc.), the leaf of foliation, on which the Hilbert space (and the quantum state) lives. In order to discuss state-operator correspondence in such a quantization scheme, one needs to map $\mathbb{R}^d$ to the cylinder $S^{d-1} \times \mathbb{R}$ using a Weyl transformation [8,15], as shown in Fig. 1. Under the Weyl transformation the dilatation $r \to e^\lambda r$ of $\mathbb{R}^d$ becomes the translation along the time direction $\tau \to \tau + \lambda$ of $S^{d-1} \times \mathbb{R}$. If the theory has conformal symmetry, we can simply relate correlators and states on $\mathbb{R}^d$ to those on $S^{d-1} \times \mathbb{R}$. Moreover, we still have the state-operator correspondence on the cylinder $S^{d-1} \times \mathbb{R}$. In particular, the state-operator correspondence on the cylinder has a nice physical interpretation, namely, the eigenstates $|\psi_n\rangle$ of the CFT quantum Hamiltonian on S^{d-1} are in one-to-one correspondence with the CFT operators, and the energy gaps δE_n of these states are proportional to the scaling dimensions Δ_n of CFT operators [8,15]:
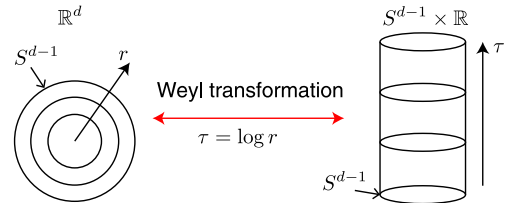
FIG. 1. Through a Weyl transformation, Euclidean flat space-time $\mathbb{R}^d$ is mapped to the manifold of cylinder $S^{d-1} \times \mathbb{R}$. As a result, a CFT on $\mathbb{R}^d$ quantized on equal radius slices can be described equivalently in terms of a CFT on $S^{d-1} \times \mathbb{R}$ quantized on equal time slices. The states defined on the $S^{d-1} \times \mathbb{R}$ have well-defined quantum numbers of SO(d) Lorentz rotation and dilatation, and thus they are in one-to-one correspondence with operators of the CFT, dubbed as state-operator correspondence.

$$\delta E_n = E_n - E_0 = \frac{v}{R}\Delta_n, \tag{4}$$

where R is the radius of sphere S^{d-1} and v is the velocity of light that is model dependent. Also the $SO(d)$ rotation symmetry of S^{d-1} is identified with the $SO(d)$ Lorentz rotation of the conformal group, so the $SO(d)$ quantum numbers of $|\psi_n\rangle$ are identical to those of CFT operators.

We emphasize that in contrast to radial quantization on $\mathbb{R}^d$, conformal symmetry is indispensable for the state-operator correspondence of radial quantization on the cylinder $S^{d-1} \times \mathbb{R}$. Therefore, observing the state-operator correspondence on the cylinder $S^{d-1} \times \mathbb{R}$ will be direct evidence for the conformal symmetry of the theory or phase transition. For $d = 2$, the cylinder $S^1 \times \mathbb{R}$ corresponds to nothing but a quantum Hamiltonian defined on a periodic chain, and there are very nice results studying the resulting state-operator correspondence [16–19]. In higher dimensions, one needs to study a quantum Hamiltonian defined on S^{d-1}; however, it is highly nontrivial for a discrete lattice model as $S^{d-1\geq 2}$ has a curvature.

B. Spherical Landau levels, fuzzy two-sphere, and lowest Landau level (LLL) projection

As originally shown by Landau, electrons moving in 2D space under a magnetic field will form completely flat bands called Landau levels, which is the key to the quantum Hall effect. Landau level quantization can be considered on any orientable manifold, and Haldane [44] first introduced Landau levels on spherical geometry to study the fractional quantum Hall physics.

For electrons moving on the surface of a radius-r sphere with a $4\pi s$ monopole ($2s \in \mathbb{Z}$) placed at the origin (Fig. 2), the Hamiltonian is

$$H_0 = \frac{1}{2M_e r^2}\Lambda_\mu^2, \tag{5}$$

where M_e is the electron's mass and $\Lambda_\mu = \partial_\mu + iA_\mu$ is the covariant angular momentum, A_μ is the gauge field of the monopole. As usual we take $\hbar = e = c = 1$. The eigenstates will be quantized into spherical Landau levels, whose energies are $E_n = [n(n+1) + (2n+1)s]/(2M_e r^2)$, with $n = 0, 1, 2, \ldots$ the Landau level index. The $(n+1)_{\text{th}}$ Landau level is $(2s + 2n + 1)$-fold degenerate, and the single particle states in each Landau level are called Landau orbitals. Assuming all interactions are much smaller than the energy gap between Landau levels, we can just consider the lowest Landau level (LLL) $n = 0$, which is $(2s + 1)$-fold degenerate. The wave functions for each Landau orbital on LLL are called monopole harmonics [45]:

$$\Phi_m(\theta, \varphi) = N_m e^{im\varphi} \cos^{s+m}\left(\frac{\theta}{2}\right)\sin^{s-m}\left(\frac{\theta}{2}\right), \tag{6}$$
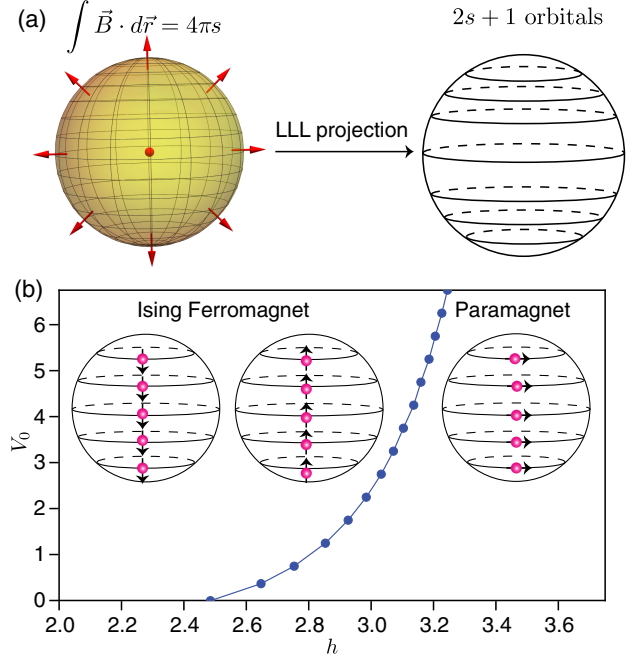
FIG. 2. (a) Schematic plot of electrons moving on a sphere in the presence of $4\pi s$ monopole. The LLL has $2s + 1$ degenerate orbitals, which form an $SO(3)$ spin-s irreducible representation. A system projected into the LLL can be equivalently viewed as a fuzzy sphere. (b) Phase diagram of the proposed model consisting of a continuous phase transition from a quantum Hall Ising ferromagnet to a disordered paramagnet.

with $m = -s, -s + 1, \ldots, s$ and $N_m = \sqrt{(2s+1)!/4\pi(s+m)!(s-m)!}$. Here (θ, φ) is the spherical coordinate.

These LLL Landau orbitals indeed form a $SO(3)$ spin-s irreducible representation. This can be understood by constructing the $SO(3)$ angular momentum operator [46],

$$L_\mu = \Lambda_\mu + s\frac{x_\mu}{r}, \tag{7}$$

which satisfies the $SO(3)$ algebra $[L_\mu, L_\nu] = i\varepsilon_{\mu\nu\rho}L_\rho$. Projecting the system into the LLL, the kinetic energy of the covariant angular momentum will be quenched, so effectively we have $L_\mu \sim s\tilde{x}_\mu/r$. ($\tilde{x}_\mu$ denotes the coordinates in the projected LLL.) As a result, the coordinates $\tilde{x}_\mu$ of electrons will not actually commute; instead we have

$$[\tilde{x}_\mu, \tilde{x}_\nu] = i\frac{r}{s}\epsilon_{\mu\nu\rho}\tilde{x}_\rho. \tag{8}$$

This defines a fuzzy two-sphere [23]. Moreover, Landau orbitals Eq. (6) are in one-to-one correspondence with states on the fuzzy two-sphere. Formally, a system defined on the LLL can be equivalently viewed as a system defined on a fuzzy two-sphere. We do not delve into details along that direction, and refer the reader to Ref. [47] for more discussions.

As is usually done in the literature, we consider the limit where the interaction strength is much smaller than the Landau level gap, so we can project the system into the LLL. Technically, this can be done by rewriting the annihilation operator $\psi(\theta, \varphi)$ on the LLL as

$$\hat{\psi}(\theta, \varphi) = \sum_{m=-s}^{s} \Phi_m^* \hat{c}_m. \tag{9}$$

$\hat{c}_m$ stands for the annihilation operator of Landau orbital m, and is independent of coordinates (θ, φ). The density operator $n(\theta, \varphi) = \psi^\dagger \psi$ can be written as

$$n(\theta, \varphi) = \sum_{m_1, m_2} \Phi_{m_1} \Phi_{m_2}^* c_{m_1}^\dagger c_{m_2}. \tag{10}$$

Any interaction can be straightforwardly (though perhaps tediously) written in the second quantized form using Landau orbital operators $c_m^\dagger, c_m$. For example, the density-density interaction $H_I = \int d^2\boldsymbol{r}_a d^2\boldsymbol{r}_b U(\boldsymbol{r}_a - \boldsymbol{r}_b) n(\boldsymbol{r}_a) n(\boldsymbol{r}_b)$ can be written as

$$H_I = \int d\Omega_a d\Omega_b U(\theta_a, \varphi_a; \theta_b, \varphi_b) n(\theta_a, \varphi_a) n(\theta_b, \varphi_b)$$

$$= \sum_{m_1, m_2, m_3, m_4} V_{m_1, m_2, m_3, m_4} c_{m_1}^\dagger c_{m_2}^\dagger c_{m_3} c_{m_4}, \tag{11}$$

where V_{m_1, m_2, m_3, m_4} can be further expanded using the so-called Haldane pseudopotential V_l [44], corresponding to the two-fermion scattering in the spin-$2s - l$ channel (see Appendix A).

In summary, the model we are working with is a fermonic Hamiltonian enclosing $2s + 1$ Landau orbitals with long-range SO(3) invariant interactions. Interestingly, all the orbitals form an SO(3) spin-s irrep. Furthermore, the length scale of the system is $\sqrt{2s + 1}$ instead of $2s + 1$ since the spatial dimension is $d = 2$, and the thermodynamic limit corresponds to taking s to infinity.

III. MODEL ON A FUZZY TWO-SPHERE

A. Hamiltonian

Here we explicitly define the model, which is spinful electrons in the LLL [48]. In spatial space, the Hamiltonian takes the form

$$H = \int d\Omega_a d\Omega_b U(\Omega_{ab}) [n^0(\theta_a, \varphi_a) n^0(\theta_b, \varphi_b)$$

$$- n^z(\theta_a, \varphi_a) n^z(\theta_b, \varphi_b)] - h \int d\Omega n^x(\theta, \varphi), \tag{12}$$

where $n^\alpha(\theta, \varphi)$ is a local density operator given by

$$n^\alpha(\theta, \varphi) = [\hat{\psi}_\uparrow^\dagger(\theta, \varphi), \hat{\psi}_\downarrow^\dagger(\theta, \varphi)] \sigma^\alpha \begin{pmatrix} \hat{\psi}_\uparrow(\theta, \varphi) \\ \hat{\psi}_\downarrow(\theta, \varphi), \end{pmatrix}, \tag{13}$$

with $\sigma^{x,y,z}$ being Pauli matrices, $\sigma^0 = I_{2\times2}$, and $U(\Omega_{ab})$ the local density-density interactions (defined below). The first term behaves like an Ising ferromagnetic interaction, while the second term is the transverse field. By projecting the Hamiltonian into the LLL, we obtain

$$H = H_{00} + H_{zz} + H_t,$$

$$H_{00} = \frac{1}{2} \sum_{m_{1,2,3,4}=-s}^{s} V_{m_1, m_2, m_3, m_4} (\mathbf{c}_{m_1}^\dagger \mathbf{c}_{m_4})(\mathbf{c}_{m_2}^\dagger \mathbf{c}_{m_3}) \delta_{m_1+m_2, m_3+m_4},$$

$$H_{zz} = -\frac{1}{2} \sum_{m_{1,2,3,4}=-s}^{s} V_{m_1, m_2, m_3, m_4} (\mathbf{c}_{m_1}^\dagger \sigma^z \mathbf{c}_{m_4})(\mathbf{c}_{m_2}^\dagger \sigma^z \mathbf{c}_{m_3})$$

$$\times \delta_{m_1+m_2, m_3+m_4},$$

$$H_t = -h \sum_{m=-s}^{s} \mathbf{c}_m^\dagger \sigma^x \mathbf{c}_m, \tag{14}$$

where $\mathbf{c}_m^\dagger = (c_{m\uparrow}^\dagger, c_{m\downarrow}^\dagger)$ is the fermion creation operator on the m_{th} Landau orbital. The parameter V_{m_1, m_2, m_3, m_4} is connected to the Haldane pseudopotential V_l by

$$V_{m_1, m_2, m_3, m_4} = \sum_l V_l (4s - 2l + 1) \begin{pmatrix} s & s & 2s - l \\ m_1 & m_2 & -m_1 - m_2 \end{pmatrix}$$

$$\times \begin{pmatrix} s & s & 2s - l \\ m_4 & m_3 & -m_3 - m_4 \end{pmatrix}, \tag{15}$$

where $\begin{pmatrix} j_1 & j_2 & j_3 \\ m_1 & m_2 & m_3 \end{pmatrix}$ is the Wigner $3j$ symbol. In this paper we only consider ultralocal density-density interactions in real space, i.e., $U(\Omega_{ab}) = g_0(1/R^2)\delta(\Omega_{ab}) + g_1(1/R^4)\nabla^2\delta(\Omega_{ab})$, and the associated Haldane pseudopotentials involve V_0, V_1 (see Appendix A). Next we set $V_1 = 1$ as energy unit and vary V_0, h to study the phase diagram.

We consider the half-filling case with the LLL filled by $N = 2s + 1$ electrons. When $h = 0$ and $V_0, V_1 > 0$, the ground state is an Ising ferromagnet that spontaneously breaks $\mathbb{Z}_2$ symmetry. In quantum Hall literature this phase is called quantum Hall ferromagnetism [49,50]. The two-fold degenerate ground states are $|\Psi_\uparrow\rangle = \prod_{m=-s}^{s} c_{m\uparrow}^\dagger |0\rangle$ and $|\Psi_\downarrow\rangle = \prod_{m=-s}^{s} c_{m\downarrow}^\dagger |0\rangle$. When $h \gg V_0, V_1$, the ground state is a trivial paramagnet that preserves Ising symmetry, $|\Psi_x\rangle = \prod_{m=-s}^{s} (c_{m\uparrow}^\dagger + c_{m\downarrow}^\dagger)|0\rangle$. Therefore, we expect a $2 + 1$D Ising transition as increasing h. The global phase diagram of the model is as shown in Fig. 2(b).

B. Symmetries and order parameter

The Hamiltonian (14) has three symmetries.
(1) Ising $\mathbb{Z}_2$ symmetry: $\mathbf{c}_m \to \sigma^x \mathbf{c}_m$.

(2) SO(3) sphere rotation symmetry: $\mathbf{c}_{m=-s,\ldots,s}$ form the spin-s representation of SO(3).

(3) Particle-hole symmetry: $\mathbf{c}_m \to i\sigma^y \mathbf{c}_m^*$, $i \to -i$.

Electric charges of fermions are gapped in the entire phase diagram (see Appendix C 1), while the Ising spins of fermions are the degrees of freedom that go through the phase transitions. Therefore, all the gapless degrees of freedom at the phase transition are charge neutral. In particular, the order parameter of the transition is a particle-hole excitation of fermions:

$$M = \sum_{m=-s}^{s} \mathbf{c}_m^\dagger \frac{\sigma^z}{2} \mathbf{c}_m. \qquad (16)$$

We emphasize an important point for the Landau level regularization of the Ising transition: the electrons are sitting on a fuzzy sphere due to the monopole, but the Ising spins are sitting on a normal sphere (for any finite $N = 2s + 1$) since they are charge neutral. This is the key difference between our Landau level regularization and the noncommutative field theory [51]; namely, the latter always has quantum fields defined on a fuzzy manifold as long as the physical volume is finite.

To further analyze the Ising transition in our system, we relate the UV symmetries of our Landau level model to the IR symmetries of the 3D Ising CFT. It is obvious we can identify the Ising $\mathbb{Z}_2$ and SO(3) sphere rotation between UV and IR. A slightly nontrivial symmetry is the particle-hole symmetry, which turns out to be the spacetime parity symmetry of 3D Ising CFT. To understand this relation, we can write an SO(3) vector,

$$n_{m=0,\pm 1}^x = \sum_{m_1=-s}^{s} (-1)^{m_1} \begin{pmatrix} s & s & 1 \\ m_1 & m-m_1 & -m \end{pmatrix} \mathbf{c}_{m_1}^\dagger \sigma^x \mathbf{c}_{m_1-m}, \qquad (17)$$

and find it transforms as

$$\begin{pmatrix} n_{m=1}^x \\ n_{m=0}^x \\ n_{m=-1}^x \end{pmatrix} \to \begin{pmatrix} 0 & 0 & -1 \\ 0 & 1 & 0 \\ -1 & 0 & 0 \end{pmatrix} \begin{pmatrix} n_{m=1}^x \\ n_{m=0}^x \\ n_{m=-1}^x \end{pmatrix}, \qquad (18)$$

under particle-hole transformation. The particle-hole acts as an improper $\mathbb{Z}_2$ of O(3), so it can be identified as the spacetime parity of the 3D Ising CFT.

C. Finite-size scaling

The phase diagram in Fig. 2(b) is obtained by the conventional finite-size scaling of the $\mathbb{Z}_2$ order parameter M in Eq. (16). We simulate $N = 2s + 1 = 8, 10, \ldots, 24$ using ED for smaller sizes ($N \leq 16$) and DMRG for larger sizes $N > 16$ (the length scale in this $2 + 1$D system is $L_x = \sqrt{N}$). At the phase transition point, the $\mathbb{Z}_2$ order
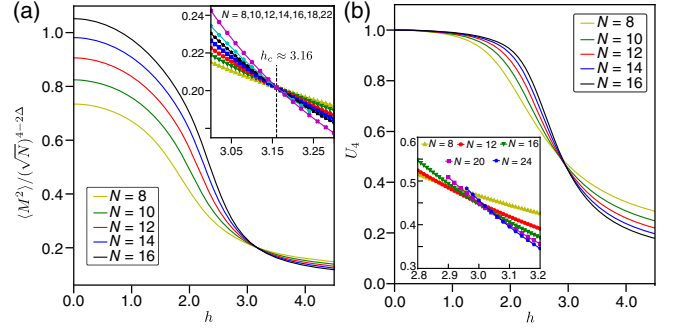
FIG. 3. (a) Finite-size scaling of order parameter $\langle M^2 \rangle / N^{2-\Delta}$. $\Delta = 0.518\,148$ is the scaling dimension of the Ising order parameter field. $N = 2s + 1$ is the number of electrons (i.e., Ising spins), hence it should be identified as space volume and the length scale is $\sim \sqrt{N}$. The rescaled order parameter perfectly crosses at the same point $h_c \approx 3.16$. (b) Plot of the RG-invariant binder cumulant U_4. The binder cumulant does not stably cross at the same point due to the large finite-size effect. We set $V_0 = 4.75$ here. The inset is a zoomed in plot.

parameter should scale as $\langle M^2 \rangle \sim L_x^{4-2\Delta} = N^{2-\Delta}$ [30], where $\Delta \approx 0.518\,148\,9$ is the scaling dimension of Ising order parameter [25,26]. Figure 3(a) depicts $\langle M^2 \rangle / N^{2-\Delta}$ with respect to the transverse field strength h of different N for $V_0 = 4.75$. All the curves nicely cross at $h_c \approx 3.16$, which we identify as the transition point. Similarly for other V_0 we identify the critical h_c and obtain the phase diagram as shown in Fig. 2(b).

We also compute the binder cumulant:

$$U_4 = \frac{3}{2} \left(1 - \frac{1}{3} \frac{\langle M^4 \rangle}{\langle M^2 \rangle^2} \right). \qquad (19)$$

U_4 is a RG-invariant quantity, and $U_4 = 1$, 0 at the thermodynamic limit corresponds to the ordered phase and disordered phase, respectively. At the phase transition U_4 will be a universal quantity related to the four-point correlator of the order parameter field σ of CFT [40]. Figure 3(b) shows U_4 with respect to the transverse field strength h for different N for $V_0 = 4.75$. Clearly, at small h the model is in the Ising ferromagnetic phase, while at large h the model is in the disordered phase. To estimate the value of binder ratio at the critical point U_4^c, we perform a detailed crossing-point analysis (Appendix B). With the data on hand, the best estimate we can give is $0.28 \leq U_4^c \leq 0.40$. It will be interesting to evaluate U_4 from conformal bootstrap and compare with our estimate [52].

In practice, for small N (as we simulate numerically), finite-size effects are inevitable. One common source is from the couplings of irrelevant operators, which are typically present in microscopic models. Tuning along the critical line in the two-dimensional parameter space (V_0, h) shown in Fig. 2(b) generically modifies the coupling strength of irrelevant operators and therefore the

magnitude of finite-size effects (while the relevant operators flow to the same fixed point). In the following section, we present the data of the state-operator correspondence at a particular point $V_0 = 4.75$, $h_c = 3.16$, where we find the finite-size effects are smallest (Appendix D).

IV. STATE-OPERATOR CORRESPONDENCE

We now turn to the central results of our paper: the state-operator correspondence of the 3D Ising transition. As explained in Sec. II A, on $S^2 \times \mathbb{R}$ the eigenstates of the quantum Hamiltonian are in one-to-one correspondence with the scaling operators of its corresponding CFT. In particular, the energy gaps of each state will be proportional to the scaling dimensions of the scaling operators [15]. Therefore, we explore energy spectra at the critical point by utilizing exact diagonalization and compare it with CFT predictions.

To match the Ising transition's energy spectra with the 3D Ising CFT's operator spectrum, we first need to rescale the energy spectrum with a nonuniversal (i.e., model- and size-dependent) numerical factor. The natural calibrator is the energy momentum tensor $T_{\mu_1\mu_2}$, a conserved operator that any local CFT possesses. For any 3D CFT, $T_{\mu_1\mu_2}$ will be a global symmetry singlet, Lorentz spin $\ell = 2$ operator with scaling dimension $\Delta_T = 3$. Our model has exact SO(3) Lorentz rotation, Ising $\mathbb{Z}_2$, and spacetime parity symmetries, so every eigenstate has well-defined quantum numbers $(\mathbb{Z}_2, P, \ell)$ of these three symmetries. The energy momentum tensor will be the lowest state in the $(\mathbb{Z}_2 = 1, P = 1, \ell = 2)$ sector. We rescale the full spectrum by setting the energy momentum tensor to exactly $\Delta_T = 3$, and then examine if the low-lying states form representations of 3D conformal symmetry up to a finite-size correction.

We analyze the low-lying spectra according to the following steps.

(1) For each $\mathbb{Z}_2 = \pm 1$ sector, we find the lowest-lying energy state (regardless of ℓ and P), and identify it as a primary state.

(2) Based on the representation theory of the 3D conformal group as summarized in Eqs. (1), (2), and (3), we enumerate the descendant states of the identified primary state and examine if all of descendant states (up to $\Delta = 7$) exist in our energy spectrum.

(3) We remove the identified conformal multiplet (i.e., primary and its descendants) from the energy spectrum, and for the remaining states we repeat steps 1 and 2.

Remarkably, we find that the lowest-lying 70 eigenstates [53] form representations of the 3D conformal symmetry up to a small finite-size correction, with no extra or missing state. This is a direct and unambiguous demonstration of the emergent conformal symmetry of the 3D Ising transition.

After verifying the emergent conformal symmetry, we further compare our scaling dimensions of the identified primary operators with the numerical conformal bootstrap data [25,26], and we find a good agreement for all of them. Table I lists all the primary operators we identify with $N = 16$ ED data. We find 12 parity-even primary operators besides the energy momentum tensor, and all of them have less than a 1.6% discrepancy from the bootstrap data [25,26]. In Appendix D we list concrete values of each conformal multiplet, as one can see the numerical accuracy is unexpectedly high, particularly given that it is from a small system size ($N = 16$ total spins): around 10 operators have relative numerical error around 3%–5.5%, and the rest of them have relative numerical error smaller than 3%. Figure 4 plots conformal multiplets of a few representative primary operators, which clearly illustrate the emergent conformal symmetry and agree well with numerical conformal bootstrap results.

A few remarks are in order. (1) We verify the emergent conformal symmetry of the 3D Ising transition by showing that the low-lying spectra of our model form representations of 3D conformal symmetry. This procedure does not rely on any input of previous knowledge such as numerical bootstrap data. (2) A spinning ($\ell > 0$) parity-even (parity-odd) primary operator can have parity-odd (parity-even) descendant operters as written in Eq. (3). This nontrivial structure from the CFT's algebra matches our ED spectrum [54]. (3) The energy momentum tensor $T_{\mu_1\mu_2}$ is a conserved operator, so it does not have any $\ell < 2$ descendant. This structure is clearly shown in our data. (4) All the parity-even primary operators that we find

TABLE I. Low-lying primary operators identified via state-operator correspondence on a fuzzy sphere with $N = 16$ electrons. The operators in the first and second row are $\mathbb{Z}_2$ odd and even operators, respectively. We highlight that two new parity-odd primary operators σ^{P-} and ϵ^{P-} are found. The conformal bootstrap data are from Ref. [26].

	σ	σ'	$\sigma_{\mu_1\mu_2}$	$\sigma'_{\mu_1\mu_2}$	$\sigma_{\mu_1\mu_2\mu_3}$	$\sigma_{\mu_1\mu_2\mu_3\mu_4}$		σ^{P-}
Bootstrap	0.518	5.291	4.180	6.987	4.638	6.113		$\cdots$
Fuzzy sphere	0.524	5.303	4.214	7.048	4.609	6.069		11.191

	ϵ	ϵ'	ϵ''	$T_{\mu\nu}$	$T'_{\mu\nu}$	$\epsilon_{\mu_1\mu_2\mu_3\mu_4}$	$\epsilon'_{\mu_1\mu_2\mu_3\mu_4}$	ϵ^{P-}
Bootstrap	1.413	3.830	6.896	3	5.509	5.023	6.421	$\cdots$
Fuzzy sphere	1.414	3.838	6.908	3	5.583	5.103	6.347	10.014
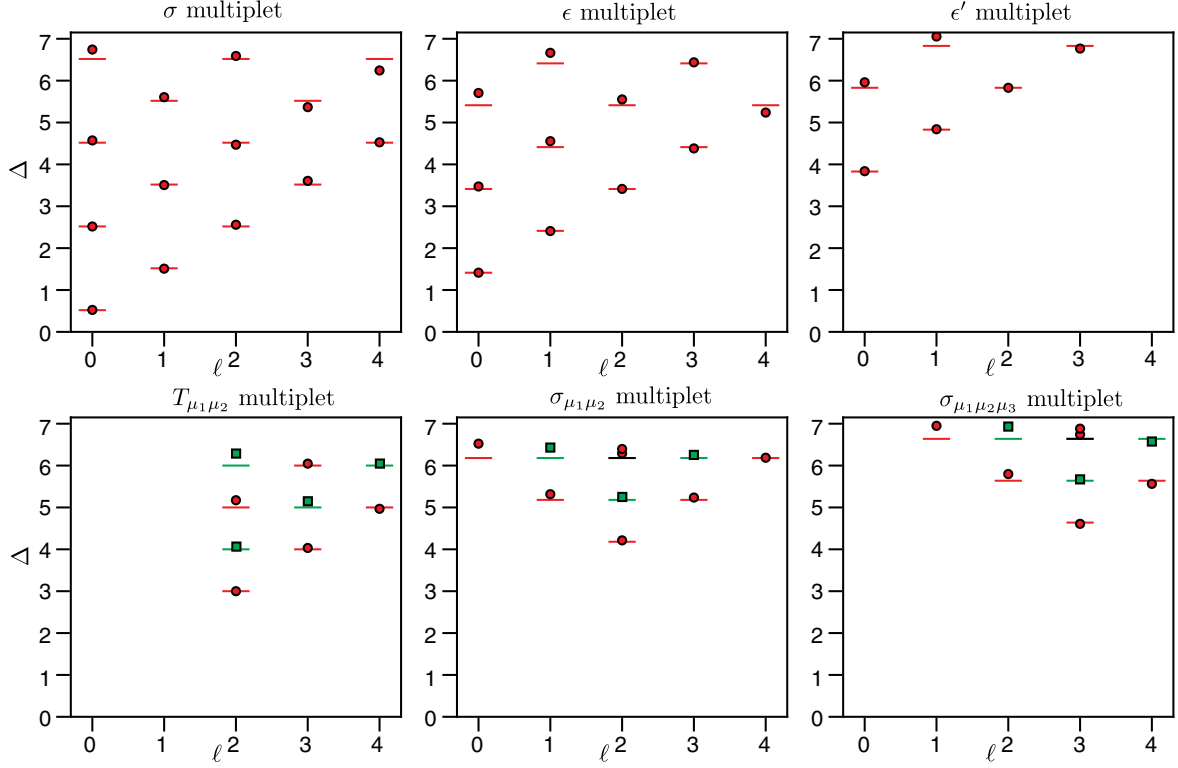
FIG. 4.   Conformal multiplet of several low-lying primary operators. Scaling dimension Δ versus Lorentz spin ℓ. We plot conformal bootstrap data with lines: lines in red are parity even, nondegenerate operators; lines in green are parity odd, nondegenerate operators; lines in black are parity even, twofold degenerate operators. Symbols are our numerical data of parity-even (red circle) and -odd (green square) operators. The discrepancy is typically more significant for the larger Δ.

have been reported in the bootstrap study of mixed correlators $\langle\sigma\sigma\sigma\sigma\rangle$, $\langle\epsilon\epsilon\epsilon\epsilon\rangle$, $\langle\sigma\sigma\epsilon\epsilon\rangle$. The mixed-correlator bootstrap study is only capable of detecting operators in the $\sigma \times \sigma$, $\epsilon \times \epsilon$ and $\sigma \times \epsilon$ operator product expansion, so it will miss $(\mathbb{Z}_2 = 1, P = 1, \text{odd}\,\ell)$ primary operators (in addition to $P = -1$ primaries). Our approach should be able to detect operators in these quantum number sectors, including the candidate of virial current [5,55], namely, the lowest primary in the $(\mathbb{Z}_2 = 1, P = 1, \ell = 1)$ sector. We do not observe any primary operators in the $(\mathbb{Z}_2 = 1, P = 1, \text{odd}\,\ell)$ sector below $\Delta = 7$, and so this gives a lower bound for the virial current candidate, which is higher than the previous estimate [14]. (5) We identify two previously unknown (parity-odd) primary operators in the $(\mathbb{Z}_2 = 1, P = -1, \ell = 0)$ and $(\mathbb{Z}_2 = -1, P = -1, \ell = 0)$ sectors with $\Delta \approx 10.01$ and $\Delta \approx 11.19$, respectively. To access $P = -1$ primary operators in the bootstrap calculation, one has to bootstrap correlation functions of the spinning operator, for example, the energy momentum tensor. Such study has only been initiated in Ref. [56], but no $P = -1$ primary has been identified by conformal bootstrap or any other methods so far. (6) In all previous lattice model studies, only several primary fields (σ, ϵ, and ϵ') were found, and their scaling dimensions are related to the critical exponents η, ν and ω [30,31].

V. SUMMARY AND DISCUSSION

We design an innovative scheme to numerically study the 3D Ising transition on the spacetime geometry $S^2 \times \mathbb{R}$, and in our calculation we find almost perfect state-operator correspondence of the 3D CFT, supporting the conjecture that the 3D Ising transition has emergent conformal symmetry. In detail, we consider the 3D Ising transition realized in a fermionic model defined on a fuzzy sphere, which we achieve by projecting spinful electrons into the lowest spherical Landau level where the spin degrees of freedom go through an order-disorder transition. We are able to identify 13 parity-even primary operators and two parity-odd primary operators, and around 60 descendant operators, in agreement with the predictions of underlying CFT within a high accuracy.

Our results have now offered a novel solution to the long-standing quest of simulating 3D CFTs on the sphere (more generally on the curved space), and even more remarkably, the finite-size effect of our model is much smaller than the conventional approach (i.e., 3D classical Ising model) used to study 3D CFTs. Therefore, our results open a new avenue for studying 3D CFTs in a microscopic way. Thanks to the state-operator correspondence on $S^2 \times \mathbb{R}$, many universal quantities such as operator product expansion coefficients, four-point correlators, and thermal

correlators of CFTs are ready to compute directly. These will lead to many insights of CFTs that are important for several purposes. For example, the thermal correlators will not only be useful for predicting experiments of $(2 + 1)$-dimensional quantum phase transitions at the finite temperature, but also help to understand the properties of quantum black holes using the AdS/CFT duality [57]. Another interesting quantity is the RG monotonic quantity F of the F theorem [36–39], which can be extracted from the quantum entanglement [58,59].

We also expect our approach can be used to tackle many open problems of the 3D CFTs. Specifically, our approach can be applied to many universalities such as $O(N)$ Wilson-Fisher transitions (i.e., XY universality) and critical gauge theories (e.g., see Ref. [60]) [61]. With a straightforward examination of the emergent conformal symmetry and a precise determination of the scaling dimensions of various primary operators, one may eventually solve the question of the conformal window of 3D critical gauge theories, a problem that has puzzled the high-energy physics and condensed matter community for decades.

In our paper the fuzzy sphere regularization is formulated using the language of lowest Landau level projection. It will be interesting to translate our formulation into the formal language of noncommutative geometry. Such perspective of the fuzzy sphere regularization may help to develop a systematic framework that is applicable to any CFT and quantum field theory (QFT) on various manifolds in arbitrary spacetime dimensions. For example, an ambitious question is, can one directly regularize the continuum QFTs on the fuzzy sphere without encountering the infamous UV infiniteness of QFTs? Indeed a similar idea was pursued decades ago in the context of noncommutative field theory [51], but was unsuccessful due to the phenomenon called UV-IR mixing. Our regularization scheme offers a new angle to this question; namely, one can introduce auxiliary fields (i.e., electrons in our model) that are living on the fuzzy sphere, and the true low-energy quantum fields of the theory (i.e., Ising spins in our model) are living on the normal sphere. We believe this way of thinking may lead to many fruitful results of CFTs and QFTs, and may reveal a new connection between physics and mathematics.

APPENDIX A: HALDANE PSEUDOPOTENTIAL ON SPHERICAL GEOMETRY

This appendix describes the expression for a general matrix element of a two-body scalar potential $V(r)$ on spherical geometry by projecting onto the lowest Landau level ($n = 0$) [44,46]. The general second-quantization form of the Hamiltonian is

$$H = \sum_{\sigma,\sigma'} \sum_{m_1,m_2,m_3,m_4=-s}^{s} c_{m_1,\sigma}^{\dagger} c_{m_2,\sigma'}^{\dagger} c_{m_3,\sigma'} c_{m_4,\sigma} \delta_{m_1+m_2,m_3+m_4}$$
$$\times \langle m_1,\sigma; m_2,\sigma'|V|m_3,\sigma'; m_4,\sigma\rangle, \quad (A1)$$

where m is orbital momentum and $\sigma = \uparrow, \downarrow$ is pseudospin index. Here we just take the interaction with the same pseudospin $\sigma = \sigma'$ as an example. The matrix element is given by

$$\langle m_1; m_2|V|m_3; m_4\rangle$$
$$= \int dr_1 \int dr_2 \Phi_{m_1}^*(r_1)\Phi_{m_2}^*(r_2)V(\mathbf{r}_1,\mathbf{r}_2)\Phi_{m_3}(r_2)\Phi_{m_4}(r_1),$$
$$(A2)$$

where Φ_m is the monopole harmonics functions defined in Eq. (6). If we expand both the initial and final state vectors in the coupled angular momentum basis, we can rewrite the two-body matrix element in the following form:

$$\langle m_1; m_2|V|m_3; m_4\rangle$$
$$= \sum_{l,l'} \langle m_1; m_2|l, m_1 + m_2\rangle \langle l', m_3 + m_4|m_4; m_3\rangle$$
$$\times \langle l, m_1 + m_2|V|l', m_3 + m_4\rangle, \quad (A3)$$

where the coefficient $\langle l, m_1 + m_2|m_1; m_2\rangle$ is the Clebsch-Gordan coefficient. $\langle l, m|V|l', m'\rangle = V_l \delta_{l,l'}$ and the pair pseudopotential V_l describes the interaction energy of a pair of electrons as a function of their pair angular momentum l [44].

To perform calculations in this paper, we use the second-quantization form of Hamiltonian Eq. (A1) with

the interaction elements shown in Eq. (A3). Since we only focus on the short-ranged interactions in real space [e.g., $\delta(\Omega_{ab}), \nabla^2\delta(\Omega_{ab})$], the choice of pseudopotential is limited to V_0, V_1. The explicit relation between the pseudopotentials and the two-body interaction potential in real space is also presented below.

1. Connection of the pseudopotential with real-space interactions

If the potential V only depends on $|\mathbf{r}_1 - \mathbf{r}_2|$ on the spherical geometry, it can be expanded in Legendre polynomials,

$$V(|\mathbf{r}_1 - \mathbf{r}_2|) = \sum_{k=0}^{\infty} U_k P_k(\cos\theta_{12}), \qquad (A4)$$

and the real-space interaction can be rewritten in terms of a new set of parameters U_k:

$$U_k = \frac{1}{2}\int_0^\pi d\theta V(|\mathbf{r}_1 - \mathbf{r}_2|)P_k(\cos\theta)\sin\theta. \quad (A5)$$

If we insert the potential form Eq. (A4) into the matrix element, we have

$$
\begin{aligned}
\langle m_1; m_2|V|m_3; m_4\rangle &= \int d\Omega_1 \int d\Omega_2 \Phi_{m_1}^*(\Omega_1)\Phi_{m_2}^*(\Omega_2)\left[\sum_k U_k \frac{1}{2k+1}\sum_{m=-k}^{k} Y_{km}^*(\Omega_1)Y_{km}(\Omega_2)\right]\Phi_{m_3}(\Omega_2)\Phi_{m_4}(\Omega_1) \\
&= \sum_k U_k \frac{1}{2k+1}\sum_{m=-k}^{k}\int d\Omega_1 \Phi_{m_1}^*(\Omega_1)\bar{Y}_{km}(\Omega_1)\Phi_{m_4}(\Omega_1)\int d\Omega_2\Phi_{m_2}^*(\Omega_2)Y_{km}(\Omega_2)\Phi_{m_3}(\Omega_2) \\
&= \sum_k U_k(-)^{6s+m_2+m_3}(2s+1)^2\begin{pmatrix} s & k & s \\ -m_1 & m_1-m_3 & m_3 \end{pmatrix}\begin{pmatrix} s & k & s \\ -m_2 & m_2-m_4 & m_4 \end{pmatrix}\begin{pmatrix} s & k & s \\ -s & 0 & s \end{pmatrix}^2. \qquad (A6)
\end{aligned}
$$

Here, for a general Wigner $3j$ coefficient, $\begin{pmatrix} s_1 & s_2 & s_3 \\ m_1 & m_2 & m_3 \end{pmatrix}$, it is nonzero only when $m_1 + m_2 + m_3 = 0$ and when s_1, s_2, s_3 together satisfy the triangle inequality, $|s_1 - s_2| \le s_3 \le s_1 + s_2$.

Through this matrix element form, one can obtain that the pseudopotential of particles in the lowest Landau level is connected with parameter U_k via

$$V_{2s-l} = \sum_{k=0}^{2s} U_k(-)^{2s_0+l}(2s+1)^2\begin{Bmatrix} l & s & s \\ k & s & s \end{Bmatrix}\begin{pmatrix} s & k & s \\ -s & 0 & s \end{pmatrix}^2, \qquad (A7)$$

where $\begin{Bmatrix} l & s & s \\ k & s & s \end{Bmatrix}$ is Wigner $6j$ coefficient.

In this paper, we only consider the short-ranged potentials as follows.

(i) For short-ranged potential $U(\Omega_{ab}) = \delta(\Omega_{ab})$, by using the expansion

$$\delta(\Omega_a - \Omega_b) = \sum_{l=0}^{\infty}\sum_{m=-l}^{l} Y_{l,m}^*(\Omega_a)Y_{l,m}(\Omega_b)$$

$$= \sum_{l=0}^{\infty}(2l+1)P_l(\cos\theta_{ab}), \qquad (A8)$$

we have $U_l = 2l + 1$. With the help of Eq. (A7), we get the pseudopotentials related to the short-ranged

potential $U(\Omega_{ab}) = \delta(\Omega_{ab})$ as

$$V_{2s-l} = \begin{cases} \frac{(2s+1)^2}{(4s+1)}, & l = 2s \\ 0, & l \ne 2s. \end{cases} \qquad (A9)$$

(ii) For short-ranged potential $U(\Omega_{ab}) = \nabla^2\delta(\Omega_{ab})$, by using the expansion

$$\nabla_a^2\delta(\Omega_a - \Omega_b) = \sum_{l=0}^{\infty}\sum_{m=-l}^{l}\nabla_a^2 Y_{l,m}^*(\Omega_a)Y_{l,m}(\Omega_b)$$

$$= \sum_{l=0}^{\infty}[-l(l+1)](2l+1)P_l(\cos\theta_{ab}), \qquad (A10)$$

we have $U_l = -l(l+1)(2l+1)$. With the help of Eq. (A7), we get the pseudopotentials related to the short-ranged potential $U(\Omega_{ab}) = \nabla_a^2\delta(\Omega_{ab})$:

$$V_{2s-l} = \begin{cases} -\frac{s(2s+1)^2}{4s+1}, & l = 2s \\ \frac{s(2s+1)^2}{4s-1}, & l = 2s - 1 \\ 0, & l < 2s - 1. \end{cases} \qquad (A11)$$

In a word, for a general two-body interaction potential on the spherical geometry $U(\Omega_{ab}) = g_0\delta(\Omega_{ab}) + g_1\nabla^2\delta(\Omega_{ab})$, one can use Eqs. (A9) and (A11) to connect with the pseudopotentials V_l as defined in Eq. (A3).

APPENDIX B: PHYSICAL OBSERVABLES ACROSS THE PHASE TRANSITION

In this appendix, we provide more detailed analysis on the finite-size scaling of physical observable M^2 and binder ratio U_4. In Fig. 5, order parameter $\langle M^2 \rangle$ is almost unchanged near the critical point $h \approx h_c$, which signals the phase transition point. In comparison, we notice that, as N increases the crossing point of U_4^c is less converged, which is not as perfect as the crossing of order parameter. In the finite-size scaling, the crossing value of the cumulant itself approaches its thermodynamic limit $U_4^c \approx 0.2849 \pm 0.0063$. And we also estimate the upper bound by the lowest value that we get in the DMRG calculation. In a word, with the data up to $N = 36$ the best estimate we can give is $U_4^c \sim (0.28, 0.40)$.

The larger uncertainty of binder ratio is likely due to the fact that the U_4 suffers a much larger finite-size effect, since at the phase transition U_4 is related to the four-point correlator of the order parameter field σ in CFT. Similar finite-size effect has also been observed in Monte Carlo simulations of 3D classical or $2 + 1$D quantum Ising transitions with much larger system size.

Additionally, we note that for the same universality defined or realized on distinct manifolds, U_4 will be generically different even in the thermodynamic limit. In principle, U_4 on the conformal manifold (e.g., R^3, $S^2 \times \mathbb{R}$) can be computed using the R^3 four-point correlator [62]. For 3D Ising transition on the nonconformal manifold such as $T^2 \times \mathbb{R}$ or T^3, which Monte Carlo usually simulates, U_4 cannot be computed using the R^3 four-point correlator.

APPENDIX C: EXCITATION GAP

1. Charge gap

In the discussion of quantum magnetism in electron systems, one preliminary question is whether or not the charge excitation gap vanishes. Here we define the charge gap as $\Delta_c(N) = E_0(N_e + 1, N) + E_0(N_e - 1, N) - 2E_0(N_e, N)$, where $E_0(N_e, N)$ is the ground state energy on N LLL orbitals by filling N_e electrons. After obtaining the charge gap on each system size, we perform a finite-size scaling to estimate the charge gap in the thermodynamic limit. As shown in Fig. 6, the charge gap at the critical point $h = h_c$ is nonzero on all system sizes, and the value in the thermodynamic limit is also finite. Thus, we conclude that the low-energy excitation is dominated by the spin excitation other than the charge excitation.

2. Spin excitation gap

In this section, we discuss the spin excitation gap. In the Ising ferromagnet ($h < h_c$), flipping a spin orientation should cost finite exchange energy, so the spin excitation gap should be nonzero. Similarly, the paramagnetic ground state $h > h_c$ is a trivial insulator, which should be separated from all other excited states by a finite energy gap. In contrast, at the critical point, the system becomes gapless, which should be distinct from the other two gapped phases. As shown in Fig. 7, we show three typical plots of excitation gap in Ising ferromagnet phase, paramagnet phase, and at the phase transition point. It is clear that the excitation gaps are finite for ferromagnet and paramagnet phase, but the system becomes gapless at the transition point $h \approx h_c$. The most interesting thing is these

FIG. 5. A finite-size scaling analysis of the Binder cumulant U_4^c at the phase transition. Each data point is determined by the crossing point on system size pair $(N, 2N)$. The analysis is according to the scaling form $U_4^c(N) = aN^{-\omega/2} + b$. Inset: example of finite-size crossing point $U_4^c(N)$ with $N = 12$ and $2N = 24$.
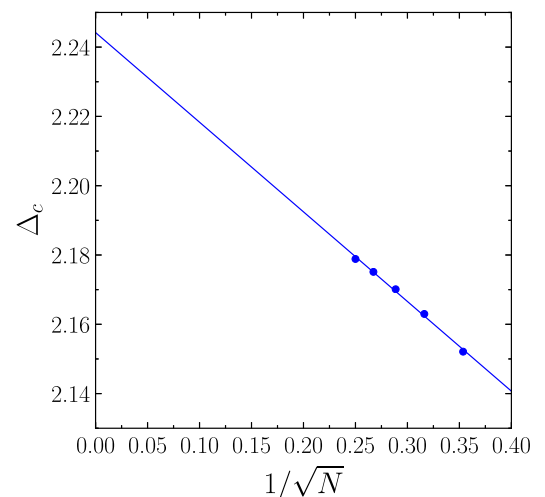
FIG. 6. Finite-size scaling of charge excitation gap at the phase transition. The charge gap is defined as $\Delta_c = E_0(N_e + 1, N) + E_0(N_e - 1, N) - 2E_0(N_e, N)$, and $E_0(N_e, N)$ is the ground state energy by filling N_e electrons.
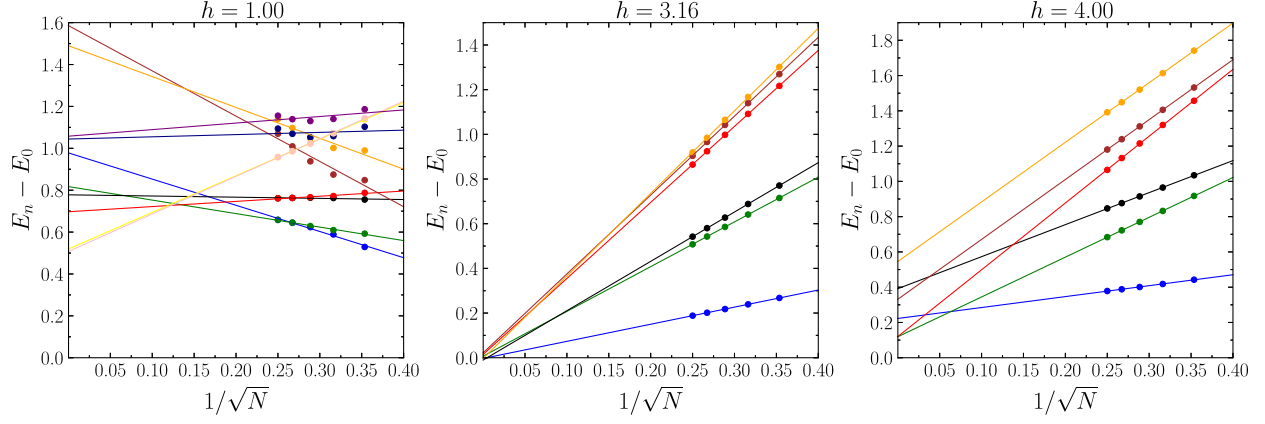
FIG. 7.   Finite-size scaling of the lowest six excitation gap of (a) quantum Hall ferromagnet at $h = 1.0 < h_c$, (b) transition point at $h = h_c$ and (c) disordered paramagnet at $h = 4.0 > h_c$.

critical excitations at finite system sizes form a characteristic conformal tower structure as discussed in the main text, which calls for a CFT description of 3D Ising criticality.

APPENDIX D: DETAILS OF NUMERICAL DATA

In this appendix, we present the data of energy spectra which are organized by the good quantum numbers and conformal multiplet of various primary fields, e.g., ϵ (Table II), ϵ' (Table III), $T_{\mu_1\mu_2}$ (Table IV), $T'_{\mu_1\mu_2}$ (Table V), $\epsilon_{\mu_1,\mu_2,\mu_3,\mu_4}$ (Table VI), σ (Table VII), σ' (Table VIII), $\sigma_{\mu_1\mu_2}$

(Table IX), and $\sigma_{\mu_1\mu_2\mu_3}$ (Table X). For comparison, we also list the results from the conformal boostrap (CB) method [25,26]. We use these data to plot Fig. 4. For the primary fields, the discrepancies are really small (<1.6%). Generally, fields with higher energies (conformal weights) have larger discrepancies, which is attributed to the finite-size effect. We add that these detailed data also give a good quantification for the numerical error without inputting other results such as numerical bootstrap. The idea is that, since the conformal symmetry predicts the integer spacings between primaries and their descendants,

TABLE II.   Conformal multiplet of ϵ.

Operator	Quantum number	CB data	$N = 16$	Errors
ϵ	$\ell = 0$	1.412 625(10)	1.413 557 66	0.066%
$\partial_\mu \epsilon$	$\ell = 1$	2.412 625(10)	2.407 764 49	0.201%
$\partial_{\mu_1}\partial_{\mu_2}\epsilon$	$\ell = 2$	3.412 625(10)	3.414 557 49	0.057%
$\Box\epsilon$	$\ell = 0$	3.412 625(10)	3.473 032 35	1.770%
$\partial_{\mu_1}\partial_{\mu_2}\partial_{\mu_3}\epsilon$	$\ell = 3$	4.412 625(10)	4.381 130 22	0.714%
$\Box\partial_\mu\epsilon$	$\ell = 1$	4.412 625(10)	4.554 378 69	3.212%
$\partial_{\mu_1}\partial_{\mu_2}\partial_{\mu_3}\partial_{\mu_4}\epsilon$	$\ell = 4$	5.412 625(10)	5.237 963 1	3.227%
$\partial_{\mu_1}\partial_{\mu_2}\Box\epsilon$	$\ell = 2$	5.412 625(10)	5.551 490 4	2.566%
$\Box^2\epsilon$	$\ell = 0$	5.412 625(10)	5.705 706 41	5.415%
$\partial_{\mu_1}\partial_{\mu_2}\partial_{\mu_3}\Box\epsilon$	$\ell = 3$	6.412 625(10)	6.437 123 03	0.382%
$\partial_{\mu_1}\Box^2\epsilon$	$\ell = 1$	6.412 625(10)	6.664 236 77	3.924%

TABLE III.   Conformal mulitplet of ϵ'.

Operator	Quantum number	CB data	$N = 16$	Errors
ϵ'	$\ell = 0$	3.829 68(23)	3.837 728 59	0.210%
$\partial_{\mu_1}\epsilon'$	$\ell = 1$	4.829 68(23)	4.839 736 17	0.208%
$\partial_{\mu_1}\partial_{\mu_2}\epsilon'$	$\ell = 2$	5.829 68(23)	5.829 182 19	0.009%
$\Box\epsilon'$	$\ell = 0$	5.829 68(23)	5.960 532 5	2.245%
$\partial_{\mu_1}\partial_{\mu_2}\partial_{\mu_3}\epsilon'$	$\ell = 3$	6.829 68(23)	6.766 176 38	0.930%
$\partial_{\mu_1}\Box\epsilon'$	$\ell = 1$	6.829 68(23)	7.054 584 33	3.293%

TABLE IV. Conformal mulitplet of $T_{\mu_1\mu_2}$.

Operator	Quantum number	Exact value	$N = 16$	Errors
$T_{\mu_1\mu_2}$	$\ell = 2$	3	3	0.000%
$\partial_{\nu_1} T_{\mu_1\mu_2}$	$\ell = 3$	4	4.032 198 19	0.805%
$\varepsilon_{\mu_2\rho\tau}\partial_\rho T_{\mu_1\mu_2}$	$\ell = 2,\ P = -1$	4	4.073 920 75	1.848%
$\partial_{\nu_1}\partial_{\nu_2} T_{\mu_1\mu_2}$	$\ell = 4$	5	4.967 341 07	0.653%
$\varepsilon_{\mu_2\rho\tau}\partial_\rho\partial_{\nu_1} T_{\mu_1\mu_2}$	$\ell = 3,\ P = -1$	5	5.146 029 26	2.921%
$\Box T_{\mu_1\mu_2}$	$\ell = 2$	5	5.172 929 63	3.459%
$\partial_{\nu_1}\Box T_{\mu_1\mu_2}$	$\ell = 3$	6	6.045 868 08	0.764%
$\varepsilon_{\mu_2\rho\tau}\partial_\rho\partial_{\nu_1}\partial_{\nu_2} T_{\mu_1\mu_2}$	$\ell = 4,\ P = -1$	6	6.062 210 26	1.037%
$\varepsilon_{\mu_2\rho\tau}\partial_\rho\Box T_{\mu_1\mu_2}$	$\ell = 2,\ P = -1$	6	6.290 745 58	4.846%

TABLE V. Conformal multiplet of $T'_{\mu_1\mu_2}$.

Operator	Quantum number	CB data	$N = 16$	Errors
$T'_{\mu_1\mu_2}$	$\ell = 2$	5.509 15(44)	5.582 714 4	1.335%
$\partial_{\nu_1} T'_{\mu_1\mu_2}$	$\ell = 3$	6.509 15(44)	6.571 379 75	0.956%
$\varepsilon_{\mu_2\rho\tau}\partial_\rho T'_{\mu_1\mu_2}$	$\ell = 2,\ P = -1,$	6.509 15(44)	6.575 578 92	1.020%
$\partial_{\mu_1} T'_{\mu_1\mu_2}$	$\ell = 1$	6.509 15(44)	6.746 395 99	3.645%

TABLE VI. Conformal mulitplet of $\epsilon_{\mu_1\mu_2\mu_3\mu_4}$.

Operator	Quantum number	CB data	$N = 16$	Errors
$\epsilon_{\mu_1\mu_2\mu_3\mu_4}$	$\ell = 4$	5.022 665(28)	5.102 994 2	1.599%
$\varepsilon_{\mu_4\rho\tau}\partial_\rho\epsilon_{\mu_1\mu_2\mu_3\mu_4}$	$\ell = 4,\ P = -1$	6.022 665(28)	6.176 846 93	2.560%
$\partial_{\mu_1}\epsilon_{\mu_1\mu_2\mu_3\mu_4}$	$\ell = 3$	6.022 665(28)	6.194 393 41	2.851%

TABLE VII. Conformal multiplet of σ.

Operator	Quantum number	CB data	$N = 16$	Errors
σ	$\ell = 0$	0.518 148 9(10)	0.524 288 57	1.185%
$\partial_\mu\sigma$	$\ell = 1$	1.518 148 9(10)	1.509 417 93	0.575%
$\Box\sigma$	$\ell = 0$	2.518 148 9(10)	2.517 221 81	0.037%
$\partial_{\mu_1}\partial_{\mu_2}\sigma$	$\ell = 2$	2.518 148 9(10)	2.559 375 03	1.637%
$\Box\partial_\mu\sigma$	$\ell = 1$	3.518 148 9(10)	3.506 353 46	0.335%
$\partial_{\mu_1}\partial_{\mu_2}\partial_{\mu_3}\sigma$	$\ell = 3$	3.518 148 9(10)	3.605 922 6	2.495%
$\Box\partial_{\mu_1}\partial_{\mu_2}\sigma$	$\ell = 2$	4.518 148 9(10)	4.470 022 81	1.065%
$\Box^2\sigma$	$\ell = 0$	4.518 148 9(10)	4.572 313 67	1.199%
$\partial_{\mu_1}\partial_{\mu_2}\partial_{\mu_3}\partial_{\mu_4}\sigma$	$\ell = 4$	4.518 148 9(10)	4.527 274 99	0.202%
$\partial_{\mu_1}\partial_{\mu_2}\partial_{\mu_3}\Box\sigma$	$\ell = 3$	5.518 148 9(10)	5.367 619 13	2.728%
$\partial_\mu\Box^2\sigma$	$\ell = 1$	5.518 148 9(10)	5.605 634 29	1.585%
$\partial_{\mu_1}\partial_{\mu_2}\partial_{\mu_3}\partial_{\mu_4}\Box\sigma$	$\ell = 4$	6.518 148 9(10)	6.242 684 67	4.226%
$\partial_{\mu_1}\partial_{\mu_2}\Box^2\sigma$	$\ell = 2$	6.518 148 9(10)	6.589 052 67	1.088%
$\Box^3\sigma$	$\ell = 0$	6.518 148 9(10)	6.743 345 14	3.455%

TABLE VIII. Conformal multiplet of σ'.

Operator	Quantum number	CB data	$N = 16$	Errors
σ'	$\ell = 0$	5.290 6(11)	5.303 466 41	0.243%
$\partial_{\mu_1}\sigma'$	$\ell = 1$	6.290 6(11)	6.277 137 85	0.214%

TABLE IX. Conformal multiplet of $\sigma_{\mu_1\mu_2}$.

Operator	Quantum number	CB data	$N = 16$	Errors
$\sigma_{\mu_1\mu_2}$	$\ell = 2$	4.180 305(18)	4.213 829 89	0.802%
$\partial_{\nu_1}\sigma_{\mu_1\mu_2}$	$\ell = 3$	5.180 305(18)	5.236 490 44	1.085%
$\partial_{\mu_1}\sigma_{\mu_1\mu_2}$	$\ell = 1$	5.180 305(18)	5.315 758 94	2.615%
$\varepsilon_{\mu_2\rho\tau}\partial_\rho\sigma_{\mu_1\mu_2}$	$\ell = 2,\, P = -1$	5.180 305(18)	5.254 153 17	1.426%
$\partial_{\nu_1}\partial_{\nu_2}\sigma_{\mu_1\mu_2}$	$\ell = 4$	6.180 305(18)	6.187 249 38	0.112%
$\varepsilon_{\mu_2\rho\tau}\partial_\rho\partial_{\nu_1}\sigma_{\mu_1\mu_2}$	$\ell = 3,\, P = -1$	6.180 305(18)	6.261 600 85	1.315%
$\partial_{\nu_1}\partial_{\mu_1}\sigma_{\mu_1\mu_2}$	$\ell = 2$	6.180 305(18)	6.291 149 75	1.794%
$\Box\sigma_{\mu_1\mu_2}$	$\ell = 2$	6.180 305(18)	6.395 951 49	3.489%
$\varepsilon_{\mu_2\rho\tau}\partial_\rho\partial_{\mu_1}\sigma_{\mu_1\mu_2}$	$\ell = 1,\, P = -1$	6.180 305(18)	6.429 991 32	4.040%
$\partial_{\mu_1}\partial_{\mu_2}\sigma_{\mu_1\mu_2}$	$\ell = 0$	6.180 305(18)	6.523 218 41	5.548%

TABLE X. Conformal multiplet of $\sigma_{\mu_1\mu_2\mu_3}$.

Operator	Quantum number	CB data	$N = 16$	Errors
$\sigma_{\mu_1\mu_2\mu_3}$	$\ell = 3$	4.638 04(88)	4.608 920 45	0.628%
$\partial_{\nu_1}\sigma_{\mu_1\mu_2\mu_3}$	$\ell = 4$	5.638 04(88)	5.563 455 84	1.323%
$\varepsilon_{\mu_3\rho\tau}\partial_\rho\sigma_{\mu_1\mu_2\mu_3}$	$\ell = 3,\, P = -1$	5.638 04(88)	5.670 445 9	0.575%
$\partial_{\mu_1}\sigma_{\mu_1\mu_2\mu_3}$	$\ell = 2$	5.638 04(88)	5.797 465 71	2.828%
$\Box\sigma_{\mu_1\mu_2\mu_3}$	$\ell = 3$	6.638 04(88)	6.740 658 48	1.546%
$\partial_{\nu_1}\partial_{\mu_1}\sigma_{\mu_1\mu_2\mu_3}$	$\ell = 3$	6.638 04(88)	6.881 822 26	3.672%
$\varepsilon_{\mu_3\rho\tau}\partial_\rho\partial_{\nu_1}\sigma_{\mu_1\mu_2\mu_3}$	$\ell = 4,\, P = -1$	6.638 04(88)	6.574 176 25	0.962%
$\varepsilon_{\mu_3\rho\tau}\partial_\rho\partial_{\mu_1}\sigma_{\mu_1\mu_2\mu_3}$	$\ell = 2,\, P = -1$	6.638 04(88)	6.931 332 76	4.418%
$\partial_{\mu_1}\partial_{\mu_2}\sigma_{\mu_1\mu_2\mu_3}$	$\ell = 1$	6.638 04(88)	6.949 009 9	4.685%

we can examine how well this is preserved in our spectrum. Based on this we can give a conservative estimate for numerical errors of primaries and low-lying descendants, which are 3% relative errors. A rigorous error analysis based on the finite-size scaling and off-critical behavior will be interesting for the future work.

Another interesting point is that we identify almost perfect state-operator correspondence in surprisingly small system sizes. In the main text, we only present the numerical data at a given system size, i.e., $N = 16$, which is the largest system size that we can reach using ED. Here, to further elucidate that the numerical findings indeed reflect the physics in the thermodynamic limit, we show the energy spectra on different system sizes. In Fig. 8, we show the energy spectra obtained on different system sizes from $N = 8$ to $N = 16$. As one can see, the energies on *all* system sizes match the prediction of 3D CFT quite well.

Finally, as we discuss in the main text, one of the most surprising aspects of the fuzzy sphere scheme is that the IR

CFT emerges in incredibly small system sizes. The best illustration is the observation that our model with only $N = 4$ spins (electrons) (Table XI) already produces six
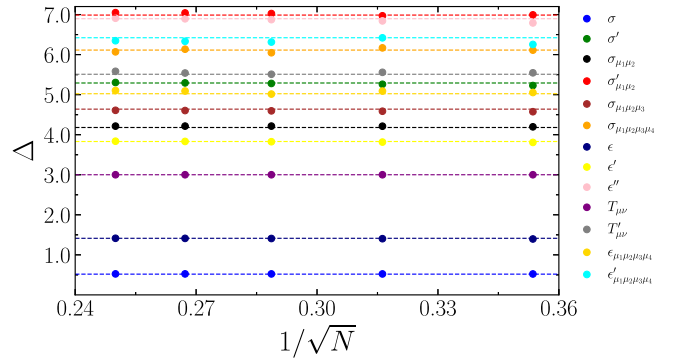
FIG. 8. The energy spectra corresponding to primary fields for various system sizes $N = 8$–16. The dashed colored lines denote the numerical values from conformal bootstrap method.

TABLE XI. The rescaled energy gaps of all states of the fuzzy sphere model with $N = 4$ spins (electrons). All the states seem to be the Ising CFT states with small finite-size corrections for most of them.

	σ	$\partial_{\mu_1}\sigma$	$\Box\sigma$	$\partial_{\mu_1}\partial_{\mu_2}\sigma$	$\partial_{\mu_1}\partial_{\mu_2}\partial_{\mu_3}\sigma$	$\partial_{\mu_1}\Box\sigma$	$\sigma_{\mu_1\mu_2}$	$\sigma_{\mu_1\mu_2\mu_3}$
Bootstrap	0.518	1.518	2.518	2.518	3.518	3.518	4.180	4.638
$N=4$	0.530	1.522	2.427	2.428	2.847	3.291	4.241	4.618
Errors	2.3%	0.3%	3.6%	3.6%	20%	6.5%	1.5%	0.4%

	ϵ	$\partial_{\mu_1}\epsilon$	$T_{\mu_1\mu_2}$	$\partial_{\mu_1}\partial_{\mu_2}\epsilon$	$\Box\epsilon$	ϵ'	$\partial_{\mu_3}T_{\mu_1\mu_2}$	$\epsilon_{\mu_2\rho\tau}\partial_\rho T_{\mu_1\mu_2}$	$\partial_{\mu_3}\partial_{\mu_4}T_{\mu_1\mu_2}$
Bootstrap	1.413	2.413	3	3.413	3.413	3.830	4	4	5
$N=4$	1.382	2.337	3	3.126	3.577	4.019	3.663	4.054	4.856
Errors	2.2%	3.1%	$\cdots$	8.4%	4.8%	4.9%	8.4%	1.4%	2.9%

primaries and the approximate conformal invariance. All calculations can be done on a laptop, where the $N = 16$ spins require around 16G memory, and the computation takes around 30 minutes on a M1 Macbook.

————————

[1] Alexander M. Polyakov, *Conformal Symmetry of Critical Fluctuations*, JETP Lett. **12**, 381 (1970).

[2] Lars Onsager, *Crystal Statistics. I. A Two-Dimensional Model with an Order-Disorder Transition*, Phys. Rev. **65**, 117 (1944).

[3] A. A. Belavin, A. M. Polyakov, and A. B. Zamolodchikov, *Infinite Conformal Symmetry in Two-Dimensional Quantum Field Theory*, Nucl. Phys. **B241**, 333 (1984).

[4] For phase transitions in 2D [5] and 4D [6] the combination of scale symmetry, Lorentz symmetry, and unitarity was shown to lead to conformal symmetry.

[5] Joseph Polchinski, *Scale and Conformal Invariance in Quantum Field Theory*, Nucl. Phys. **B303**, 226 (1988).

[6] Anatoly Dymarsky, Zohar Komargodski, Adam Schwimmer, and Stefan Theisen, *On Scale and Conformal Invariance in Four Dimensions*, J. High Energy Phys. 10 (2015) 171.

[7] Philippe Francesco, Pierre Mathieu, and David Sénéchal, *Conformal Field Theory*, Graduate Texts in Contemporary Physics (Springer, New York, 1997).

[8] J. L. Cardy, *Conformal Invariance and Universality in Finite-Size Scaling*, J. Phys. A **17**, L385 (1984).

[9] M. Weigel and W. Janke, *Universal Amplitude-Exponent Relation for the Ising Model on Sphere-like Lattices*, Europhys. Lett. **51**, 578 (2000).

[10] Youjin Deng and Henk W. J. Blöte, *Conformal Invariance of the Ising Model in Three Dimensions*, Phys. Rev. Lett. **88**, 190602 (2002).

[11] M. Billó, M. Caselle, D. Gaiotto, F. Gliozzi, M. Meineri, and R. Pellegrini, *Line Defects in the 3D Ising Model*, arXiv:1304.4110.

[12] Catarina Cosme, J. M. Viana Parente Lopes, and João Penedones, *Conformal Symmetry of the Critical 3D Ising Model inside a Sphere*, J. High Energy Phys. 08 (2015) 022.

[13] Michael Schuler, Seth Whitsitt, Louis-Paul Henry, Subir Sachdev, and Andreas M. Läuchli, *Universal Signatures of Quantum Critical Points from Finite-Size Torus Spectra: A Window into the Operator Content of Higher-Dimensional Conformal Field Theories*, Phys. Rev. Lett. **117**, 210401 (2016).

[14] Simão Meneses, João Penedones, Slava Rychkov, J. M. Viana Parente Lopes, and Pierre Yvernay, *A Structural Test for the Conformal Invariance of the Critical 3D Ising Model*, J. High Energy Phys. 04 (2019) 115.

[15] J. L. Cardy, *Universal Amplitudes in Finite-Size Scaling: Generalisation to Arbitrary Dimensionality*, J. Phys. A **18**, L757 (1985).

[16] H. W. J. Blöte, John L. Cardy, and M. P. Nightingale, *Conformal Invariance, the Central Charge, and Universal Finite-Size Amplitudes at Criticality*, Phys. Rev. Lett. **56**, 742 (1986).

[17] Ian Affleck, *Universal Term in the Free Energy at a Critical Point and the Conformal Anomaly*, in *Current Physics—Sources and Comments*, Vol. 2 (Elsevier, New York, 1988). pp. 347–349.

[18] Ashley Milsted and Guifre Vidal, *Extraction of Conformal Data in Critical Quantum Spin Chains Using the Koo-Saleur Formula*, Phys. Rev. B **96**, 245105 (2017).

[19] Yijian Zou, Ashley Milsted, and Guifre Vidal, *Conformal Data and Renormalization Group Flow in Critical Quantum Spin Chains Using Periodic Uniform Matrix Product States*, Phys. Rev. Lett. **121**, 230402 (2018).

[20] In mathematics the problem of tiling a sphere is called spherical tiling or spherical polyhedron.

[21] R. C. Brower, G. T. Fleming, and H. Neuberger, *Lattice Radial Quantization: 3D Ising*, Phys. Lett. B **721**, 299 (2013).

[22] R. C. Brower, G. T. Fleming, A. D. Gasbarro, D. Howarth, T. G. Raben, Chung-I Tan, and E. S. Weinberg, *Radial Lattice Quantization of 3D ϕ^4 Field Theory*, Phys. Rev. D **104**, 094502 (2021).

[23] John Madore, *The Fuzzy Sphere*, Classical Quantum Gravity **9**, 69 (1992).

[24] Matteo Ippoliti, Roger S. K. Mong, Fakher F. Assaad, and Michael P. Zaletel, *Half-Filled Landau Levels: A Continuum and Sign-Free Regularization for Three-Dimensional Quantum Critical Points*, Phys. Rev. B **98**, 235108 (2018).

[25] David Poland, Slava Rychkov, and Alessandro Vichi, *The Conformal Bootstrap: Theory, Numerical Techniques, and Applications*, Rev. Mod. Phys. **91**, 015002 (2019).

[26] D. Simmons-Duffin, *The Lightcone Bootstrap and the Spectrum of the 3D Ising CFT*, J. High Energy Phys. 03 (2017) 086.

[27] Vyacheslav S. Rychkov and Alessandro Vichi, *Universal Constraints on Conformal Operator Dimensions*, Phys. Rev. D **80,** 045006 (2009).

[28] S. El-Showk, M. F. Paulos, D. Poland, S. Rychkov, D. Simmons-Duffin, and A. Vichi, *Solving the 3D Ising Model with the Conformal Bootstrap*, Phys. Rev. D **86,** 025022 (2012).

[29] Filip Kos, David Poland, David Simmons-Duffin, and Alessandro Vichi, *Precision Islands in the Ising and O(N) Models*, J. High Energy Phys. 08 (2016) 036.

[30] Martin Hasenbusch, *Finite Size Scaling Study of Lattice Models in the Three-Dimensional Ising Universality Class*, Phys. Rev. B **82,** 174433 (2010).

[31] Alan M. Ferrenberg, Jiahao Xu, and David P. Landau, *Pushing the Limits of Monte Carlo Simulations for the Three-Dimensional Ising Model*, Phys. Rev. E **97,** 043301 (2018).

[32] Andrea Pelissetto and Ettore Vicari, *Critical Phenomena and Renormalization-Group Theory*, Phys. Rep. **368,** 549 (2002).

[33] We note that Ref. [34] claimed a proof of the conformal invariance of 3D Ising transition, but it is unclear if the proof is correct; see the comment in Appendix B of arXiv: 1802.02319.

[34] Bertrand Delamotte, Matthieu Tissier, and Nicolás Wschebor, *Scale Invariance Implies Conformal Invariance for the Three-Dimensional Ising Model*, Phys. Rev. E **93,** 012144 (2016).

[35] Yu Nakayama, *Scale Invariance vs Conformal Invariance*, arXiv:1302.0884.

[36] Horacio Casini, Marina Huerta, and Robert C. Myers, *Towards a Derivation of Holographic Entanglement Entropy*, J. High Energy Phys. 05 (2011) 036.

[37] Daniel L. Jafferis, Igor R. Klebanov, Silviu S. Pufu, and Benjamin R. Safdi, *Towards the F-Theorem: $\mathcal{N} = 2$ Field Theories on the Three-Sphere*, J. High Energy Phys. 06 (2011) 102.

[38] Robert C. Myers and Aninda Sinha, *Holographic c-Theorems in Arbitrary Dimensions*, J. High Energy Phys. 01 (2011) 125.

[39] H. Casini and M. Huerta, *Renormalization Group Running of the Entanglement Entropy of a Circle*, Phys. Rev. D **85,** 125016 (2012).

[40] Daniel Berkowitz and George Fleming, *Critical Three-Dimensional Ising Model on Spheriods from the Conformal Bootstrap*, arXiv:2110.12109.

[41] Slava Rychkov, *EPFL Lectures on Conformal Field Theory in $D \geq 3$ Dimensions*, SpringerBriefs in Physics (Springer, New York, 2017).

[42] Here we are talking about primary operators under the global conformal symmetry $SO(d + 1, 1)$. For 2D CFTs one usually talks about primary operators under Virasoro symmetries, and the global conformal primaries are called quasiprimaries.

[43] The conformal multiplet of a conserved operator is called a short multiplet.

[44] F. D. M. Haldane, *Fractional Quantization of the Hall Effect: A Hierarchy of Incompressible Quantum Fluid States*, Phys. Rev. Lett. **51,** 605 (1983).

[45] Tai Tsun Wu and Chen Ning Yang, *Dirac Monopole without Strings: Monopole Harmonics*, Nucl. Phys. **B107,** 365 (1976).

[46] Martin Greiter, *Landau Level Quantization on the Sphere*, Phys. Rev. B **83,** 115129 (2011).

[47] Kazuki Hasebe, *Hopf Maps, Lowest Landau Level, and Fuzzy Spheres*, SIGMA **6,** 071 (2010).

[48] The spin degree of freedom should be thought of as a pseudospin as it does not couple to the Zeeman field of the magnetic monopole.

[49] S. L. Sondhi, A. Karlhede, S. A. Kivelson, and E. H. Rezayi, *Skyrmions and the Crossover from the Integer to Fractional Quantum Hall Effect at Small Zeeman Energies*, Phys. Rev. B **47,** 16419 (1993).

[50] Steven M. Girvin, *Spin and Isospin: Exotic Order in Quantum Hall Ferromagnets*, Phys. Today **53,** No. 6, 39 (2000).

[51] Michael R. Douglas and Nikita A. Nekrasov, *Noncommutative Field Theory*, Rev. Mod. Phys. **73,** 977 (2001).

[52] For models on the nonconformal manifold such as $T^2 \times \mathbb{R}$ or T^3, which Monte Carlo usually simulates, U_4 cannot be computed using the R^3 four-point correlator from conformal bootstrap.

[53] We target the lowest 100 eigenstates using ED without explicitly imposing the value of ℓ, and we only look at states with $\ell \leq 4$ which roughly contains 70 states.

[54] To recall, the UV particle-hole symmetry becomes the spacetime parity symmetry of the IR CFT.

[55] Strictly speaking, virial current refers to an operator with scaling dimension $\Delta = 2$. If such an operator exists, one may have a theory that is scale invariant but not conformal invariant.

[56] Anatoly Dymarsky, Filip Kos, Petr Kravchuk, David Poland, and David Simmons-Duffin, *The 3D Stress-Tensor Bootstrap*, J. High Energy Phys. 02 (2018) 164.

[57] A CFT at finite temperature on boundary is dual to a black hole of quantum gravity in the bulk.

[58] Igor R. Klebanov, Silviu S. Pufu, Subir Sachdev, and Benjamin R. Safdi, *Entanglement Entropy of 3-D Conformal Gauge Theories with Many Flavors*, J. High Energy Phys. 05 (2012) 036.

[59] Horacio Casini, Marina Huerta, Robert C. Myers, and Alexandre Yale, *Mutual Information and the F-Theorem*, J. High Energy Phys. 10 (2015) 003.

[60] Zhenjiu Wang, Michael P. Zaletel, Roger S. K. Mong, and Fakher F. Assaad, *Phases of the $(2 + 1)$ Dimensional SO(5) Nonlinear Sigma Model with Topological Term*, Phys. Rev. Lett. **126,** 045701 (2021).

[61] A guiding principle for the model design will be kinematical properties such as symmetries and anomalies. Here we start with spinful fermions, whose maximal spin symmetry is SU(2). We further add interactions that break SU(2) down to the anomaly-free Ising $\mathbb{Z}_2$ symmetry. Similarly, for other transitions one can start with N-component fermions, and consider various interactions that break the maximal SU(N) symmetry to the desired symmetries.

[62] An approximate R^3 four-point correlator can be reconstructed using the data from conformal bootstrap.